LETTERS
PUBLISHED ONLINE: 17 JUNE 2012 | DOI: 10.1038/NNANO.2012.95
nature nanotechnology

# Valley polarization in $MoS_2$ monolayers by optical pumping

Hualing Zeng[1†], Junfeng Dai[2,1†], Wang Yao[1,3], Di Xiao[4] and Xiaodong Cui[1*]

**Most electronic devices exploit the electric charge of electrons, but it is also possible to build devices that rely on other properties of electrons. Spintronic devices, for example, make use of the spin of electrons[1,2]. Valleytronics is a more recent development that relies on the fact that the conduction bands of some materials have two or more minima at equal energies but at different positions in momentum space[3–5]. To make a valleytronic device it is necessary to control the number of electrons in these valleys, thereby producing a valley polarization[6–11]. Single-layer $MoS_2$ is a promising material for valleytronics because both the conduction and valence band edges have two energy-degenerate valleys at the corners of the first Brillouin zone[12]. Here, we demonstrate that optical pumping with circularly polarized light can achieve a valley polarization of 30% in pristine monolayer $MoS_2$. Our results, and similar results by Mak *et al.*[13], demonstrate the viability of optical valley control and valley-based electronic and optoelectronic applications in $MoS_2$ monolayers.**

In many crystalline materials, it often happens that the conduction-band minima and valence-band maxima are located at degenerate and inequivalent valleys in momentum space. The valley index can be regarded as a discrete degree of freedom for low-energy carriers, which is robust against smooth deformation and low-energy phonons because of the large valley separation in momentum space. To make use of the valley index as an information carrier, the crucial step is to identify a process in which the valley carriers respond differently to external stimuli. Recently, a simple scheme based on inversion symmetry breaking has been proposed to realize the manipulation of the valley index through electric, magnetic and optical means[5,11]. In particular, it was shown that inversion symmetry breaking can lead to contrasting circular dichroism in different $k$-space regions, which takes the extreme form of contrasting optical selection rules at the high symmetry points of the Brillouin zone[11]. This enables a valley-dependent interplay of electrons with light of different circular polarizations, in analogy to the spin-dependent optical activities in semiconductors such as GaAs.

Here, we report our observation of selective photoexcitation of the degenerate valleys by circularly polarized optical pumping in $MoS_2$ monolayers, an emerging multi-valley two-dimensional semiconductor with remarkable optical and transport properties[14,15]. Bulk $MoS_2$ has a hexagonal-crystal layered structure with a covalently bonded S–Mo–S hexagonal quasi-two-dimensional network packed by weak van der Waals forces. Previous studies have shown that, with a decrease in thickness, $MoS_2$ crosses over from being an indirect-bandgap semiconductor (with multiple layers) to a direct-bandgap semiconductor (as a monolayer)[15,16]. The direct bandgap is in the visible frequency range (~1.9 eV) and is therefore ideal for optical applications, with both conduction and valence band edges located at the K (K′) points of the two-dimensional hexagonal Brillouin zone. In addition to the changes to its electronic structure, $MoS_2$ thin film also undergoes a structural change, as outlined in Fig. 1a. The inversion symmetry present in bulk and in thin films with an even number of layers is explicitly broken in thin films with an odd number of layers, giving rise to a valley-contrasting optical selection rule[11,12,17], where the inter-band transitions in the vicinity of the K (K′) point couple exclusively to right (left)-handed circularly polarized light $\sigma+$ ($\sigma-$) (Fig. 1). The direct-bandgap transition at the two degenerate valleys, together with this valley-contrasting selection rule, suggest that one can optically generate and detect valley polarizations in a $MoS_2$ monolayer.

Our main result is summarized in the following. We find that in $MoS_2$ monolayers, the photoluminescence has the same helicity in its circularly polarized component as the excitation laser, a signature of optically pumped valley polarization. Below 90 K, a high photoluminescence circular polarization is observed, which decays with temperature. The photoluminescence polarization shows no dependence on the in-plane magnetic field. The absence of the Hanle effect is a strong indicator that the polarized photoluminescence arises from the polarization of the valley rather than spin, as the former cannot be rotated by the magnetic field. Moreover, in $MoS_2$ bilayers, we find that photoluminescence from $MoS_2$ bilayers is unpolarized under the same excitation conditions, consistent with the presence of inversion symmetry.

$MoS_2$ flakes, shown representatively in Fig. 2a, were mechanically exfoliated from $SiO_2$/silicon substrates using sticky tape in a manner similar to the technique used to produce graphene sheets. The monolayer, bilayer and multilayer flakes could be identified by two characteristic Raman modes: the in-plane vibrational $E^1_{2g}$ mode and the out-of-plane vibrational $A_{1g}$ mode around 400 $cm^{-1}$ (ref. 14). Following ref. 14, we labelled the sample thickness according to the frequency difference between the $E^1_{2g}$ and $A_{1g}$ modes: $\Delta\omega = 19\ cm^{-1}$ indicating monolayers and $\Delta\omega = 21\ cm^{-1}$ bilayers (Fig. 2b). The layer assignment was confirmed by atomic force microscopy (AFM). Photoluminescence spectra around 1.9 eV, corresponding to excitons from the direct inter-band transition[18], were also used as a monolayer and bilayer indicator from the transition from indirect- to direct-gapped semiconductor, as illustrated in refs 15,16.

The polarization-sensitive photoluminescence measurement was carried out using a confocal-like microscopic set-up. The collimated backscattering light was passed through a broadband $1/4\lambda$ wave plate, a beam-displacing prism to separate the light beam into two orthogonally polarized beams and a depolarizer, and was then focused to two spots at the entrance slit of the monochromator equipped with a charge-coupled device (CCD) camera. The

[1]Physics Department, The University of Hong Kong, Pokfulam road, Hong Kong, China, [2]Department of Physics, South University of Science and Technology of China, Shenzhen 518055, China, [3]Center of Theoretical and Computational Physics, The University of Hong Kong, Hong Kong, China, [4]Materials Science and Technology Division, Oak Ridge National Laboratory, Oak Ridge, Tennessee 37831, USA, †These authors contributed equally to this work.
*e-mail: xdcui@hku.hk



© 2012 Macmillan Publishers Limited. All rights reserved.

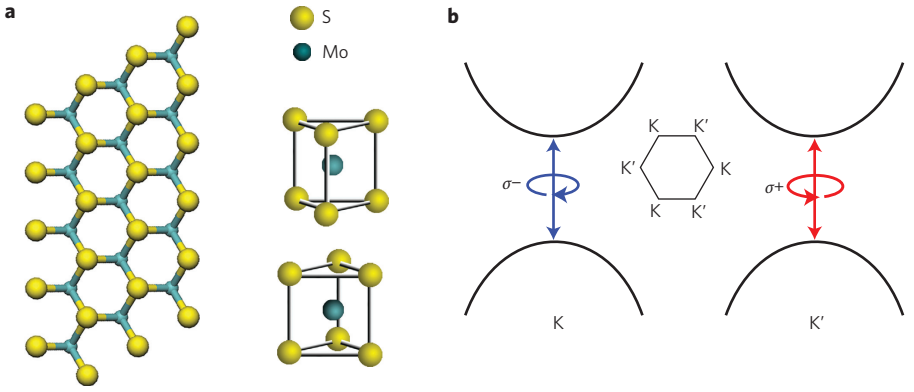


**Figure 1 | Schematic of $MoS_2$ monolayer and optical selection rules at K(K′) point. a**, Schematic of $MoS_2$ monolayer structure (left) and bulk unit cell (right), clearly showing the spatial inversion symmetry breaking in monolayers. **b**, Schematic of proposed valley-dependent selection rules at K and K′ points in crystal momentum space: left (right)-handed circularly polarized light $\sigma+$ ($\sigma-$) only couples to the band-edge transition at K (K′) points for the sake of angular moment conservation and time reversal symmetry.

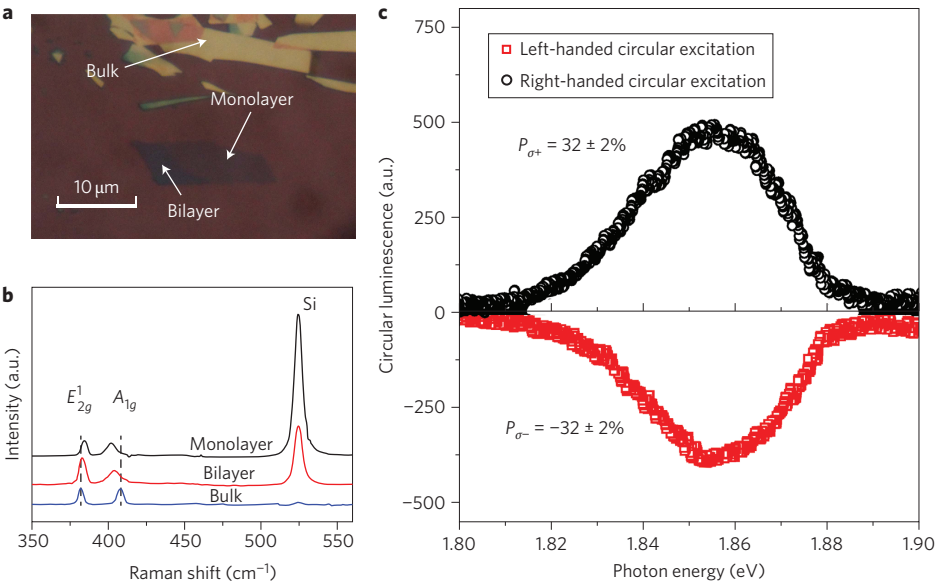


**Figure 2 | Polarization-sensitive photoluminescence spectra from $MoS_2$ monolayers. a**, Representative optical image of $MoS_2$ monolayer, bilayer and thin-film flakes. **b**, Characteristic Raman spectra from different $MoS_2$ flakes (monolayer, bilayer and thin film), showing an in-plane vibrational $E^1_{2g}$ mode and an out-of-plane vibrational $A_{1g}$ mode around 400 cm$^{-1}$. **c**, Polarization resolved luminescence spectra under circularly polarized excitation from a HeNe laser at 1.96 eV and 10 K. Circular polarizations of $P = 32 \pm 2\%$ and $-32 \pm 2\%$ are observed along the out-of-plane direction with right- and left-handed circular excitation, respectively.

polarization resolved spectrum could then be obtained by analysing the two branches of dispersion on the CCD. (For details regarding the set-up, see Supplementary Information.)

Figure 2c presents the circularly polarized luminescence spectra of a pristine $MoS_2$ monolayer, which peak around 1.9 eV with right- and left-handed circularly polarized excitation (HeNe laser, 1.96 eV) at a near-resonant condition at $T = 10$ K. The luminescence corresponds to a direct inter-band transition at the K (K′) valley. The helicity of the luminescence exactly follows that of the excitation light. In other words, the right-handed circularly polarized excitation generates right-handed luminescence, and the left-handed circularly polarized excitation generates left-handed luminescence. To characterize the circular component in the luminescence spectra, we define the degree of circular polarization

$$P = \frac{I(\sigma+) - I(\sigma-)}{I(\sigma+) + I(\sigma-)}$$

where $I(\sigma\pm)$ is the intensity of the left (right)-handed circular component. For perfectly circularly polarized light, $P = 1$ ($\sigma+$) or $-1$ ($\sigma-$) (for details see Supplementary Information). The luminescence spectra demonstrate a symmetric polarization for excitation with opposite helicities: $P = 0.32$ under $\sigma+$ excitation and $P = -0.32$ under $\sigma-$ excitation for the most representative $MoS_2$ monolayer out of four samples that gave values of $P = \pm 0.23$, $\pm 0.25$, $\pm 0.28$ and $\pm 0.32$ under $\sigma\pm$ excitation, respectively, at 10 K. This behaviour is fully expected under the mechanism of the valley-dependent optical selection rule. As well as the unpolarized background, there is also a linearly polarized component, and the linear polarization shifts by $\sim 25^\circ$ between $\sigma+$ and $\sigma-$ excitation. If one switches the excitation light to a higher energy at 2.33 eV, no polarization can be observed in the luminescence spectra. We note that the valley selection rule is valid in the vicinity of the K (K′) point[11,12], whereas the optical transition with 2.33 eV occurs far away from the K points in band dispersion.



© 2012 Macmillan Publishers Limited. All rights reserved.

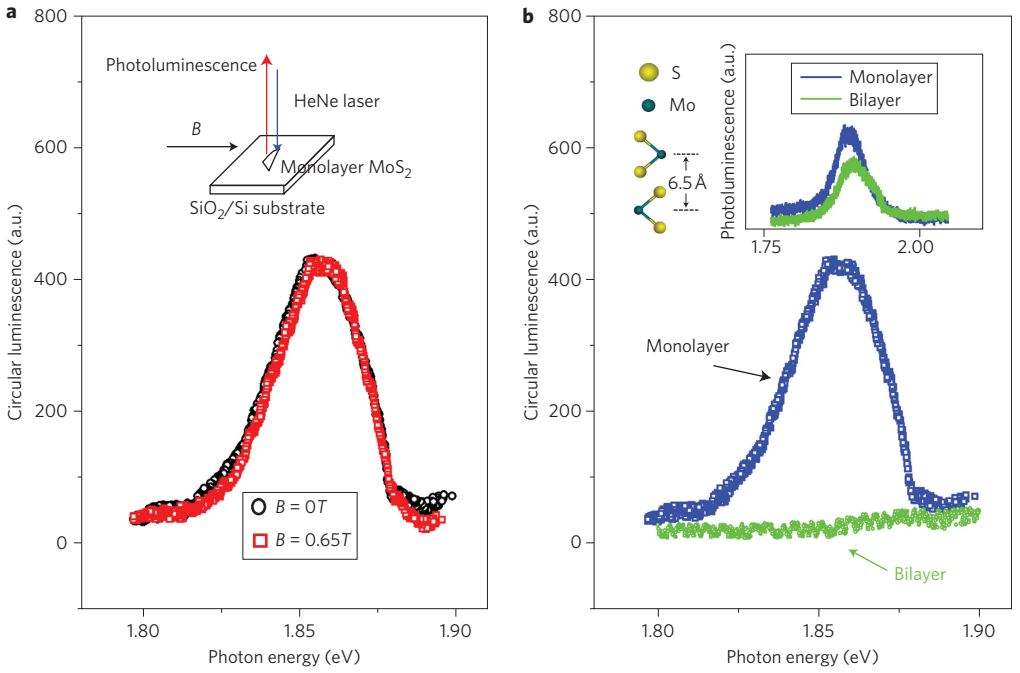


**Figure 3 | Photoluminescence under an in-plane magnetic field and from bilayers. a**, Circularly polarized components of luminescence spectra at zero magnetic field (black) and under an in-plane magnetic field of 0.65*T* (red). The two curves overlap within the resolution of the apparatus. **b**, Upper left inset: schematic of a $MoS_2$ bilayer unit cell. Upper right inset: photoluminescence spectra of monolayer (blue) and bilayer (green) $MoS_2$ under the same conditions (base temperature, 10 K; 0.2 mW linearly polarized excitation at 1.96 eV). The intensity of the bilayer luminescence is slightly weaker than that of the monolayer. Main panel: circularly polarized components of luminescence spectra from $MoS_2$ bilayers (green) and monolayers (blue) under circular excitation at 1.96 eV and 10 K. Negligible circular polarization is observed for the $MoS_2$ bilayers.

In many semiconductor systems such as GaAs bulk and heterostructures, the circular polarization of luminescence from circularly polarized excitation originates from electron (hole) spin polarization as a result of the spin-dependent optical selection rule[19,20]. This mechanism can be excluded here by examining the change in the photoluminescence spectra in an in-plane magnetic field (Fig. 3a). With a non-zero in-plane *g*-factor, spin polarization will precess about the in-plane magnetic field, and the time average of the spin projected along the *z*-axis will be found at $S_z = \int_0^\tau S_{Z0} \exp(-t/\tau_S) \cos(g\mu_B Bt/\hbar)dt$, where $S_{Z0}$ is the initial spin along the *z*-axis, $\tau_S$ is the spin relaxation time, $\mu_B$ is the Bohr magneton and $\tau$ is the lifetime of the photoexcited carriers. Consequently, the polarization of the luminescence under continuous-wave excitation should follow

$$P(B) \approx \frac{P(B=0)}{1+(g\mu_B B\tau_S/\hbar)^2}$$

where $P(B=0)$ is the polarization of the luminescence without the magnetic field. This is the well-known Hanle effect. If we assume that the spin relaxation time $\tau_S$ is of approximately the same order as the photocarrier lifetime $\tau \approx 10$ ps (ref. 21), then the polarization $P(B=0.65T)$ will drop to a few per cent of $P(B=0)$. As shown in Fig. 3a, however, there is no visible difference between the photoluminescence polarization at zero field and in an in-plane field of $B=0.65T$. Therefore, spin polarization cannot explain the polarized photoluminescence observed here. Instead, this magnetic-field-independent photoluminescence polarization is a fully expected consequence of valley polarization through the valley-dependent selection rule; because the in-plane magnetic field does not couple to the valley index, the valley polarization cannot be rotated by the magnetic field, so no Hanle effect can be observed.

Further evidence for attributing the polarized photoluminescence in monolayers to the valley-dependent optical selection rule can be found from a comparison with photoluminescence spectra from $MoS_2$ bilayers (Fig. 3b). The intensity of the luminescence in bilayers is relatively weaker than that of monolayers, with the striking difference being that the circular polarization of luminescence from bilayers is negligible under the same conditions. This difference can be easily understood: the polarized photoluminescence is a consequence of the valley-dependent optical selection rule arising from inversion symmetry breaking in $MoS_2$ monolayers with $D_{3h}^1$ symmetry[12]. In contrast, $MoS_2$ bilayers are composed of two structurally identical monolayers stacking with hexagonal symmetry (the sulphur atoms in one layer sit directly upon/below the molybdenum atoms in the other) and have $D_{6h}^4$ symmetry. Inversion symmetry is preserved in the bilayer unit cell, so the valley-dependent selection rule is not allowed in bilayers[11]. If the excitation power is increased above $1 \times 10^5$ W cm$^{-2}$, circularly polarized photoluminescence is observed in bilayers, suggesting that the heating effects could induce structural anisotropy and consequently break the inversion symmetry in the bilayer.

Figure 4 displays the typical temperature dependence of the circular polarization of luminescence from monolayers under circularly polarized excitation. The circular polarization has a flat plateau at ~31% below 90 K, then dramatically drops with increasing temperature. The small temperature dependence of the polarization at low temperatures implies that the inter-valley scattering ($K \leftrightarrow K'$) results mainly from scattering at grain boundaries and atomically sharp deformations. Because the sample is a natural mining product, abundant impurities and vacancies presumably provide inter-valley scattering centres and populate conduction electrons at the energetically degenerate K and K′ valleys. The linearly polarized component of luminescence also suggests possible coherent mixing of the two valleys.



© 2012 Macmillan Publishers Limited. All rights reserved.

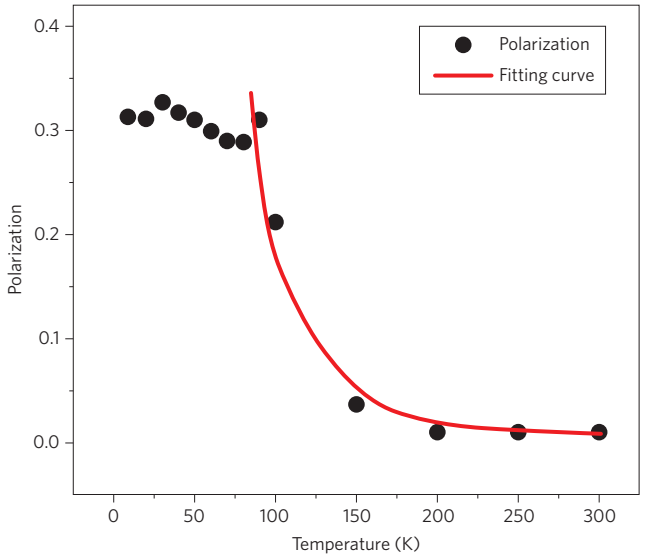


**Figure 4 | Degree of circular polarization *P* as a function of temperature.** The fitting curve (red), assuming an inter-valley scattering proportional to the phonon population, gives a phonon energy of ~240 $cm^{-1}$.

As the temperature increases above 90 K, the circularly and linearly polarized components of the luminescence spectra gradually decrease, which is an indicator of phonons dominating the inter-valley scattering at high temperatures. The steady-state photoluminescence polarization is inversely proportional to the valley scattering rate $\gamma_v$. Phonons near the K points of the Brillouin zone can directly supply the momentum change for inter-valley scattering. In such a situation, the valley scattering rate is proportional to the population of these phonons—$\gamma_v \propto \exp(-E_K/k_BT)$—where $E_K$ is the phonon energy near the K points. The solid curve in Fig. 4 is a fit assuming an $\exp(-E_K/k_BT)$ dependence, from which we extract $E_K \approx 240\ cm^{-1}$, consistent with the acoustic phonon energy near the K point reported in the bulk and monolayers[22,23]. To obtain a complete understanding and microscopic pictures of valley depolarization in this material, further systematic experimental and theoretical investigations will be required.

In summary, we have observed circularly polarized luminescence from $MoS_2$ monolayers under circularly polarized excitation. The circular polarization originates from the contrasting selection rules for optical transitions in the K and K′ valleys. It provides us with a viable tool with which to generate and detect valley polarization in $MoS_2$ monolayers, which may form the basis for developing integrated valleytronic and spintronic applications on this platform, with strong valley–spin coupling[12].

Received 16 April 2012; accepted 10 May 2012;
published online 17 June 2012

## References

1. Wolf, S. A. *et al.* Spintronics: a spin-based electronics vision for the future. *Science* **294,** 1488–1495 (2001).
2. Zutic, I., Fabian, J. & Das Sarma, S. Spintronics: fundamentals and applications. *Rev. Mod. Phys.* **76,** 323–410 (2004).
3. Rycerz, A., Tworzydlo, J. & Beenakker, C. W. J. Valley filter and valley valve in graphene. *Nature Phys.* **3,** 172–175 (2007).
4. Shkolnikov, Y. P., De Poortere, E. P., Tutuc, E. & Shayegan, M. Valley splitting of AlAs two-dimensional electrons in a perpendicular magnetic field. *Phys. Rev. Lett.* **89,** 226805 (2002).
5. Xiao, D., Yao, W. & Niu, Q. Valley-contrasting physics in graphene: magnetic moment and topological transport. *Phys. Rev. Lett.* **99,** 236809 (2007).
6. Zhu, Z., Collaudin, A., Fauque, B., Kang, W. & Behnia, K. Field-induced polarization of Dirac valleys in bismuth. *Nature Phys.* **8,** 89–94 (2012).
7. Gunawan, O. *et al.* Valley susceptibility of an interacting two-dimensional electron system. *Phys. Rev. Lett.* **97,** 186404 (2006).
8. Tombros, N. *et al.* Quantized conductance of a suspended graphene nanoconstriction. *Nature Phys.* **7,** 697–700 (2011).
9. Low, T. & Guinea, F. Strain-induced pseudomagnetic field for novel graphene electronics. *Nano Lett.* **10,** 3551–3554 (2010).
10. Gunlycke, D. & White, C. T. Graphene valley filter using a line defect. *Phys. Rev. Lett.* **106,** 136806 (2011).
11. Yao, W., Xiao, D. & Niu, Q. Valley-dependent optoelectronics from inversion symmetry breaking. *Phys. Rev. B* **77,** 235406 (2008).
12. Xiao, D., Liu, G. B., Feng, W., Xu, X. D. & Yao, W. Coupled spin and valley physics in monolayers of $MoS_2$ and other group-VI dichalcogenides. *Phys. Rev. Lett.* **108,** 196802 (2012).
13. Mak, K. F., He, K., Shan, J. & Heinz, T. F. Control of valley polarization in monolayer $MoS_2$ by optical helicity. *Nature Nanotech.* http://dx.doi.org/10.1038/nnano.2012.96 (2012).
14. Lee, C. *et al.* Anomalous lattice vibrations of single- and few-layer $MoS_2$. *ACS Nano* **4,** 2695–2700 (2010).
15. Mak, K. F., Lee, C., Hone, J., Shan, J. & Heinz, T. F. Atomically thin $MoS_2$: a new direct-gap semiconductor. *Phys. Rev. Lett.* **105,** 136805 (2010).
16. Splendiani, A. *et al.* Emerging photoluminescence in monolayer $MoS_2$. *Nano Lett.* **10,** 1271–1275 (2010).
17. Cao, T., Feng, J., Shi, J., Niu, Q. & Wang, E. $MoS_2$ as an ideal material for valleytronics: valley-selective circular dichroism and valley Hall effect. Preprint at http://arxiv.org/abs/1112.4013 (2011).
18. Frindt, R. F. & Yoffe, A. D. Physical properties of layer structures: optical properties and photoconductivity of thin crystals of molybdenum disulphide. *Proc. R. Soc. Lond. A* **273,** 69–83 (1963).
19. Parsons, R. R. Band-to-band optical pumping in solids and polarized photoluminescence. *Phys. Rev. Lett.* **23,** 1152–1154 (1969).
20. Dyakonov, M. I. Introduction to spin physics in semiconductors. *Physica E* **35,** 246–250 (2006).
21. Korn, T., Heydrich, S., Hirmer, M., Schmutzler, J. & Schuller, C. Low-temperature photocarrier dynamics in monolayer $MoS_2$. *Appl. Phys. Lett.* **99,** 102109 (2011).
22. Wakabayashi, N., Smith, H. G. & Nicklow, R. M. Lattice dynamics of hexagonal $MoS_2$ studied by neutron scattering. *Phys. Rev. B* **12,** 659–663 (1975).
23. Jiménez Sandoval, S., Yang, D., Frindt, R. F. & Irwin, J. C. Raman study and lattice dynamics of single molecular layers of $MoS_2$. *Phys. Rev. B* **44,** 3955–3962 (1991).

## Acknowledgements

The authors thank Bairen Zhu, Lu Xie, Dongmei Deng, J.Q. Ning, C.C. Zheng and S.J. Xu for technical assistance. H.Z., J.D., X.C. and W.Y. were supported by the Research Grant Council (HKU10/CRF/08, HKU701810P, HKU706412P) and the University Grant Council (AoE/P-04/08 and SEG_CUHK06) of the government of HKSAR. D.X. was supported by the US Department of Energy, Office of Basic Energy Sciences, Materials Sciences and Engineering Division.

## Author contributions

X.C. and W.Y. conceived the project. X.C., H.Z. and J.D. designed the experiments. H.Z. and J.D. performed the experiments. W.Y. and D.X. provided theoretical support. All authors discussed the results and co-wrote the paper.

## Additional information

The authors declare no competing financial interests. Supplementary information accompanies this paper at www.nature.com/naturenanotechnology. Reprints and permission information is available online at http://www.nature.com/reprints. Correspondence and requests for materials should be addressed to X.C.



© 2012 Macmillan Publishers Limited. All rights reserved.